Electrically polarized amorphous sodo-niobate film competing with crystalline lithium niobate second order optical response

*Lara Karam, Frédéric Adamietz, Dominique Michau, Claudia Gonçalves, Myungkoo Kang, Rashi Sharma, G. Senthil Murugan, Thierry Cardinal, Evelyn Fargin, Vincent Rodriguez, Kathleen A. Richardson, Marc Dussauze**

L. Karam, F. Adamietz, Prof. V. Rodriguez, Dr. M. Dussauze
Institut des Sciences Moléculaires, UMR 5255 CNRS
Université de Bordeaux
351 Cours de la Libération, 33405, Talence Cedex, France
E-mail : marc.dussauze@u-bordeaux.fr

D. Michau, Dr. T. Cardial, Prof. E. Fargin
Institut de Chimie de la Matière Condensée de Bordeaux, UMR 5026 CNRS
Université de Bordeaux
87 avenue du Dr. Albert Schweitzer, 33600 Pessac Cedex, France

Dr. C. Gonçalves, Dr. M. Kang, Dr. R. Sharma, Prof. K. A. Richardson
CREOL, College of Optics and Photonics, Department of Materials Science and Engineering
University of Central Florida
Orlando, FL 32816, United States

Dr. G. S. Murugan
Optoelectronics Research Centre
University of Southampton
Southampton SO17 1BJ, United Kingdom

Keywords: nonlinear optical materials, amorphous thin films, poling

The design of active optical devices integrating second-order nonlinear (SONL) optical responses typically relies on the use of dielectric crystalline materials such as lithium niobate (LN) or semi-conductors such as GaAs. Despite high SONL susceptibilities, these materials present important geometry constrains inherent to their crystalline nature limiting the complexity of the designed photonic systems. Conversely, amorphous materials are versatile optical media compatible with broad platform designs possessing a wide range of optical properties attributable to their composition flexibility. Demonstrated here for the first time in an amorphous inorganic material, we report a magnitude of SONL optical susceptibility ($\chi^{(2)}$ =29 pm/V at 1.06 µm) comparable to that of LN single crystal. By using a thermo-electrical imprinting process, fine control of the induced uniaxial anisotropy is demonstrated at the micrometer scale. This work paves the way for the future design of integrated nonlinear

photonic circuits based on amorphous inorganic materials enabled by the spatially selective and high SONL optical susceptibility of these promising and novel glass materials.

Research efforts towards the realization of efficient integrated photonic circuits (IPCs) where active and passive optical components are combined on a single chip, have expanded over the past decade. While this technology continues to mature, there remains significant challenges associated with planar material optical function and multi-material integration. The design of complex photonic structures requires a spatial control at widely varying length scales (from micrometer to centimeter) and the merging of multiple optical and chemical functionalities (for sensing devices). A promising platform for IPCs is silicon based[1] due to the very high refractive index (RI) difference between the silicon waveguide and its cladding (air or silicon oxide) which induces strong confinement of light allowing unprecedented small bend radii (down to 1 μm); such attributes can thus minimize the resulting component's footprint. Thanks to this confinement, efficient third order optical processes like stimulated Raman scattering have been observed in silicon waveguides[1]. However, as many active optical devices rely on second order nonlinear (SONL) optical processes rather than third, silicon cannot meet this demand as it is centrosymmetric and thus possesses a $\chi^{(2)}$ of zero. Efforts to modify this intrinsic behavior have been reported showing that one can break silicon's centrosymmetry and induce a $\chi^{(2)}$ as high as 15 pm/V in a straight waveguide by depositing a straining layer on the waveguide's surface.[2] Another important platform for IPCs is lithium niobate (LN).[3] LN exhibits good optical transparency spanning from the visible to mid-infrared as well as a strong SONL response ($\chi^{(2)}_{zzz}$=55 pm/V for the single crystal grown from the congruent melt)[4] making it a material of choice for active optical devices for telecommunication. Traditional approaches to form waveguides in bulk LN through processes

like Ti^+ diffusion have been shown to result in low RI differences and thus don't allow for complex structures. Unlike silicon, LN crystal is not isotropic thus enabling a strong SONL optical response yet creating possible geometry restrictions in the realization of certain devices. Several methods can be used to circumvent this problem. One is to use LN thin films on insulators (LNOI) making possible the design of ridge and wire waveguides exhibiting appreciable RI difference.[3] Quasi-phase matching (QPM) for frequency conversion has been achieved on periodically grooved[5] dry etched or periodically poled[6] (based on domain inversion) LNOI waveguides with good results. Another strategy employed is to use the LN platform for its SONL optical properties but to rely on an easily patterned material to form the guiding structure. Amorphous materials are good candidates for this task. Electro-optical microring resonators and Mach-Zehnder interferometers have been realized on a LNOI platform with a patterned chalcogenide thin film waveguide.[7] Compared to their crystalline counterparts, amorphous materials are more flexible and versatile as they are compatible with a range of forming processes and their optical properties can be tailored by tuning their composition.

Since many active optical devices rely on SONL properties and since glass is isotropic, its use is often limited to passive components such as waveguides. It is well known that breaking the centrosymmetry of glass by heating the sample under a strong voltage followed by cooling back down before removal of the DC field (or thermal poling) can result in the formation of a stable SONL optical susceptibility at the glass' surface. This process was first observed in fused silica[8] and has since been extended to many different glass families including silicate,[9] heavy metal oxides,[10–12] chalcogenides[13] among others. It can also be applied to chromophores containing polymer[14–16]; hence, this constitutes a field of research beyond the scope of this paper but such applicability to multiple systems highlights the versatility of the approach. Thermal poling used as an imprinting process (employing a patterned electrode) has resulted in the demonstration of superb spatial control of a stable SONL susceptibility at the

micrometer scale in different bulk glasses.[17,18] To date, limited efforts to extend this effect to amorphous thin films suitable for integrated planar structures have been shown.[19–21] While interesting findings have resulted from these studies, no amorphous inorganic material (in bulk or thin film form) has to date exhibited SONL susceptibility levels of sufficient magnitude to replace LN-based structures.

This work describes the patterning of SONL susceptibility of amorphous thin film in the binary system Nb_2O_5-Na_2O, demonstrating its potential as a promising candidate system with a range of physical and optical properties suited to IPCs. To the best of our knowledge, only one other group has reported the RF sputtering synthesis of amorphous $NaNbO_3$ thin films.[22] Here, we focus on one thin film composition containing 10 at.% of sodium with films prepared by radiofrequency (RF) sputtering. The cross section of these films as investigated by scanning electron microscopy (SEM) (**Figure 1a**) shows excellent thickness uniformity, good adhesion to the borosilicate microscope slide substrate with no evidence of delamination. The 1.83±0.02 µm thick film appears homogenous at this scale, with no sign of porosity nor other microstructural defects which could lead to light scattering. The composition homogeneity throughout the thickness of the film has been confirmed by secondary ion mass spectroscopy (SIMS) measurements (**Figure 1b**) and the film's amorphous nature is validated by the x-ray diffraction (XRD) diffractogram (**Figure 1c**). The optical properties of the film are shown **Figure 1d** through **1f**. The film's refractive index dispersion has been quantified by two different techniques (ellipsometry and refractometry) and measurements from both are in good agreement; these data were successfully fitted using a Sellmeier equation[23] across a large spectral window (0.5 to 4.5 µm) where the film is transmissive. The film exhibits a refractive index of 2.046±0.005 at 1.064 µm which is comparable to that reported for amorphous Nb_2O_5.[24] The transparency domain, reconstructed from transmission measurements in the visible and reflection measurements in the infrared due to the substrate's absorption (Figure 1e and 1f), spans from 0.4 to 5 µm exhibiting

comparable optical transparency to that shown by LN.[3] These measurements also confirm the absence of light scattering in the whole spectral region investigated, consistent with no evidence of nanocrystallinity in the film.

An efficient thermo-electrical imprinting process on ionic bulk glasses is characterized by a depletion of mobile cations under the conductive parts of the electrode. The next two figures clearly illustrate how this process is successfully transferred to amorphous thin films in the present work. The principle of the micro-poling treatment is illustrated in **Figure 2a**. Here, the electrode is comprised of an indium tin oxide (ITO) thin film that is ablated by laser irradiation to form alternating patterned regions of conductive and nonconductive zones. In a manner similar to that used in previous studies on bulk glasses,[17] Raman mapping (**Figure 2b** through **2d**) of the band centered at 850 cm^{-1} (Figure 2c) was used to track the sodium distribution on the surface of the patterned film. This band is attributed to Nb-O stretching modes where the oxygen is involved in an ionic bond with sodium. We observe a decrease of this band for regions of the thin film under the conductive zones of the electrode (zone 2) confirming the departure of sodium with the electrical field. Furthermore, a concurrent evolution of the signature associated with molecular oxygen (mapping of the band at 1550 cm^{-1}, Figure 2d is seen, as observed in prior efforts where it was shown that this band is associated with an electronic or ionic conduction that compensates for the departure of positive charges.[25,26] Both maps show evidence of homogenous structural rearrangement of the film, corresponding to the regions of the electrode's pattern correlating and illustrating the spatial precision of the imprinting process. The localization, the geometry and the magnitude of the SONL optical response are discussed in **Figure 3**. Here, the second harmonic generation (SHG), evidence of the SONL optical response in the film, was probed under specular reflection conditions using a confocal microscope. The sample is oriented so that the linearly polarized incident light is perpendicular to the imprinted line (along the X axis, see Figure 2a for the orientation of the sample). The SHG signal is analyzed along the same

polarization orientation thus the term $\chi^{(2)}_{xxx}$ of the SONL susceptibility tensor is probed. The SHG response is confined (c.f. **Figure 3a**) to regions where the sodium concentration gradient is the strongest (i.e. at the edge of the conductive part of the electrode). It is maximal at the border of the sodium-rich/sodium-depleted zones and decreases by three orders of magnitude over less than three microns.

The SHG response in the patterned domains is largest when the sample is oriented as shown (corresponding to 0 or 180° positions on the polar plot **Figure 3b**). When the orientation of the sample turns the signal gradually decays following a square cosine function to reach a complete extinction when the imprinted line is parallel to the incident light polarization (corresponding to 90 or 270 ° on the polar plot). This directional variation shows the uniaxial geometry of this response and the rigorous geometry control of the SONL susceptibility.

In order to quantify the magnitude of the SONL optical susceptibility obtained using our imprinting process on these sodo-niobate amorphous films, we have measured the SHG as a function of the incident power and compared it to that of a reference (**Figure 3c**). The reference material used is a bulk lithium niobate single crystal grown from a congruent melt. Both measurements were made under the exact same experimental conditions. Here, the incident and analyzed polarizations were along the bulk single crystal's c axis so that only the strongest coefficient of the SONL susceptibility tensor of the crystalline reference ($\chi^{(2)}_{zzz}$=55±6 pm/V)[4] was probed. The SHG signal's quadratic dependence were fitted on the basis of the classical theoretical expression of the SHG intensity as a function of the incident power.[27] From these data, we extracted the magnitude of the thin film's SONL susceptibility using the ratio between the two quadratic law fitting coefficients, taking into account the different refractive indices, and incorporating a correction for the surface's reflection losses (all details are given in the supporting information). Employing this protocol, the SONL susceptibility micro-localized at the sodium-rich/sodium-depleted (on a scale of 3 µm) frontier of these amorphous sodo-niobate films was determined to be 29±4 pm/V. After

demonstrating such accurate and spatially precise control of the second order optical properties for these electrically polarized amorphous optical thin films, the next step is naturally to progress toward the fabrication of features such as nonlinear optical amorphous waveguides which would be important geometries in the design of a planar optical devices. The lines that we have imprinted on the films are 5 mm long and a similar SHG response has been measured over their whole length (±10 % in intensity). Hence, we can reasonably prospect to apply this technique to induce a second order optical susceptibility over long distances which could be of interest for the design of an electro-optical waveguide. To achieve quasi phase patching conditions (QPM), a waveguide could be poled with a comb-like electrode (similar to the one used here[28]) on its side to obtain periodically alternating SONL active and non-active domains. Now, if a similar comb-like electrode were to be put on the other side of the waveguide but with a spatial offset, inverted domains could be formed along the waveguide. According to the index dispersion of these niobate amorphous films (Figure 1), the coherence length varies from 9 to 25 µm for wavelengths ranging from 1.5 to 3 µm; hence, the accuracy of the imprinting process demonstrated in this study denotes the feasibility to pattern the SONL properties of these niobate amorphous materials within this scale range.

In conclusion, we have synthesized and characterized the properties of amorphous sodo-niobate thin film materials. A thermo-electrical imprinting process was applied to these high optical quality thin films extending to thin films previously observed in bulk poling mechanisms. An unprecedented high SONL optical susceptibility for an amorphous inorganic material, on the order of magnitude of that of crystalline LN was demonstrated and quantified in side-by-side evaluation of both materials The fine control of the localization and the geometry of the resulting SONL response enabled through the use of patterned electrode, has demonstrated the potential viability of these materials in future devices. The fabrication flexibility guaranteed by the amorphous nature of the sodo-niobate thin film combined with

an easy protocol to induce microscale, local uniaxial anisotropies with $\chi^{(2)}$ values, competing with a crystalline LN, opens vast new opportunities for the design and manufacturing of planar photonic architectures for the visible through mid-infrared spectral region.

Supporting Information

Supporting information is available from Wiley Online Library or from the author.

Acknowledgments

The authors would like to thank Mikhail Klimov, at the Material Characterization Facility (MCF) at UCF for conducting the SIMS measurements and Pieter Kik (CREOL) for giving access to his ellipsometer, Eric Lebraud, at the ICMCB common characterization service for carrying the XRD measurements. The authors also appreciate the helpful discussions with Juejun Hu at MIT for his relevant suggestions related to photonic device design constraints and requirements. The authors gratefully acknowledge the financial support of: IdEx Bordeaux (Cluster of Excellence LAPHIA and the allocated grant referred to as ANR-10-IDEX-03-03), the IdEx Bordeaux Visiting Scholar program, and the CNRS project EMERGENCE @INC2019. This project has received funding from the European Union's Horizon 202 research program under the Marie Skłodowska-Curie grant agreement No 823941 (FUNGLASS).

Competing Interests statements:

The authors declare no competing interests.

Received:
Revised:
Published online:

References

[1] W. Bogaerts, P. De Heyn, T. Van Vaerenbergh, K. De Vos, S. Kumar Selvaraja, T. Claes, P. Dumon, P. Bienstman, D. Van Thourhout, R. Baets, *Laser & Photon. Rev.* **2012**, *6*, 47.

[2] R. S. Jacobsen, K. N. Andersen, P. I. Borel, J. Fage-Pedersen, L. H. Frandsen, O. Hansen, M. Kristensen, A. V. Lavrinenko, G. Moulin, H. Ou, C. Peucheret, B. Zsigri, A. Bjarklev, *Nature* **2006**, *441*, 199.

[3] A. Boes, B. Corcoran, L. Chang, J. Bowers, A. Mitchell, *Laser & Photonics Reviews* **2018**, *12*, 1700256.

[4] V. G. Dmitriev, G. G. Gurzadyan, D. N. Nikogosyan, *Handbook of Nonlinear Optical Crystals*, Springer Berlin Heidelberg, Berlin, Heidelberg, **1997**.

[5] C. Wang, X. Xiong, N. Andrade, V. Venkataraman, X.-F. Ren, G.-C. Guo, M. Lončar, *Opt. Express* **2017**, *25*, 6963.

[6] L. Chang, Y. Li, N. Volet, L. Wang, J. Peters, J. E. Bowers, *Optica* **2016**, *3*, 531.

[7] A. Rao, A. Patil, J. Chiles, M. Malinowski, S. Novak, K. Richardson, P. Rabiei, S. Fathpour, *Opt. Express* **2015**, *23*, 22746.

[8] R. A. Myers, N. Mukherjee, S. R. Brueck, *Optics Letters* **1991**, *16*, 1732.

[9] F. C. Garcia, I. C. S. Carvalho, E. Hering, W. Margulis, B. Lesche, *Applied Physics Letters* **1998**, *72*, 3252.

[10] B. Ferreira, E. Fargin, B. Guillaume, G. Le Flem, V. Rodriguez, M. Couzi, T. Buffeteau, L. Canioni, L. Sarger, G. Martinelli, Y. Quiquempois, H. Zeghlache, L. Carpentier, *Journal of Non-Crystalline Solids* **2003**, *332*, 207.

[11] K. Tanaka, A. Narazaki, K. Hirao, *Opt. Lett.* **2000**, *25*, 251.

[12] V. Nazabal, E. Fargin, J. J. Videau, G. Le Flem, A. Le Calvez, S. Montant, E. Freysz, A. Ducasse, M. Couzi, *Journal of Solid State Chemistry* **1997**, *133*, 529.

[13] M. Guignard, V. Nazabal, F. Smektala, J.-L. Adam, O. Bohnke, C. Duverger, A. Moréac, H. Zeghlache, A. Kudlinski, G. Martinelli, Y. Quiquempois, *Adv. Funct. Mater.* **2007**, *17*, 3284.

[14] S. K. Yesodha, C. K. Sadashiva Pillai, N. Tsutsumi, *Progress in Polymer Science* **2004**, *29*, 45.

[15] L. Dalton, in *Polymers for Photonics Applications I* (Ed.: K.-S. Lee), Springer Berlin Heidelberg, Berlin, Heidelberg, **2002**, pp. 1–86.

[16] P. Labbé, A. Donval, R. Hierle, E. Toussaere, J. Zyss, *Comptes Rendus Physique* **2002**, *3*, 543.

[17] M. Dussauze, V. Rodriguez, F. Adamietz, G. Yang, F. Bondu, A. Lepicard, M. Chafer, T. Cardinal, E. Fargin, *Advanced Optical Materials* **2016**, *4*, 929.

[18] A. Lepicard, F. Adamietz, V. Rodriguez, K. Richardson, M. Dussauze, *Opt. Mater. Express* **2018**, *8*, 1613.

[19] Y. Quiquempois, A. Villeneuve, D. Dam, K. Turcotte, J. Maier, G. Stegeman, S. Lacroix, *Electronics Letters* **2000**, *36*, 733.

[20] M. Dussauze, A. Malakho, E. Fargin, J. P. Manaud, V. Rodriguez, F. Adamietz, B. Lazoryak, *Journal of Applied Physics* **2006**, *100*, 013108.

[21] A. S. K. Tong, F. Bondu, G. Senthil Murugan, J. S. Wilkinson, M. Dussauze, *Journal of Applied Physics* **2019**, *125*, 015104.

[22] V. Lingwal, N. S. Panwar, *Journal of Applied Physics* **2003**, *94*, 4571.

[23] J. D. Musgraves, J. Hu, L. Calvez, *Springer Handbook of Glass*, **2019**.

[24] Ö. D. Coşkun, S. Demirel, G. Atak, *Journal of Alloys and Compounds* **2015**, *648*, 994.

[25] T. Cremoux, M. Dussauze, E. Fargin, T. Cardinal, D. Talaga, F. Adamietz, V. Rodriguez, *The Journal of Physical Chemistry C* **2014**, *118*, 3716.

[26] M. Dussauze, V. Rodriguez, A. Lipovskii, M. Petrov, C. Smith, K. Richardson, T. Cardinal, E. Fargin, E. I. Kamitsos, *J. Phys. Chem. C* **2010**, *114*, 12754.

[27] R. W. Boyd, *Nonlinear Optics*, Elsevier, **2003**.

[28] P. Mackwitz, M. Rüsing, G. Berth, A. Widhalm, K. Müller, A. Zrenner, *Appl. Phys. Lett.* **2016**, *108*, 152902.

[29] N. Bloembergen, P. S. Pershan, *Phys. Rev.* **1962**, *128*, 606.

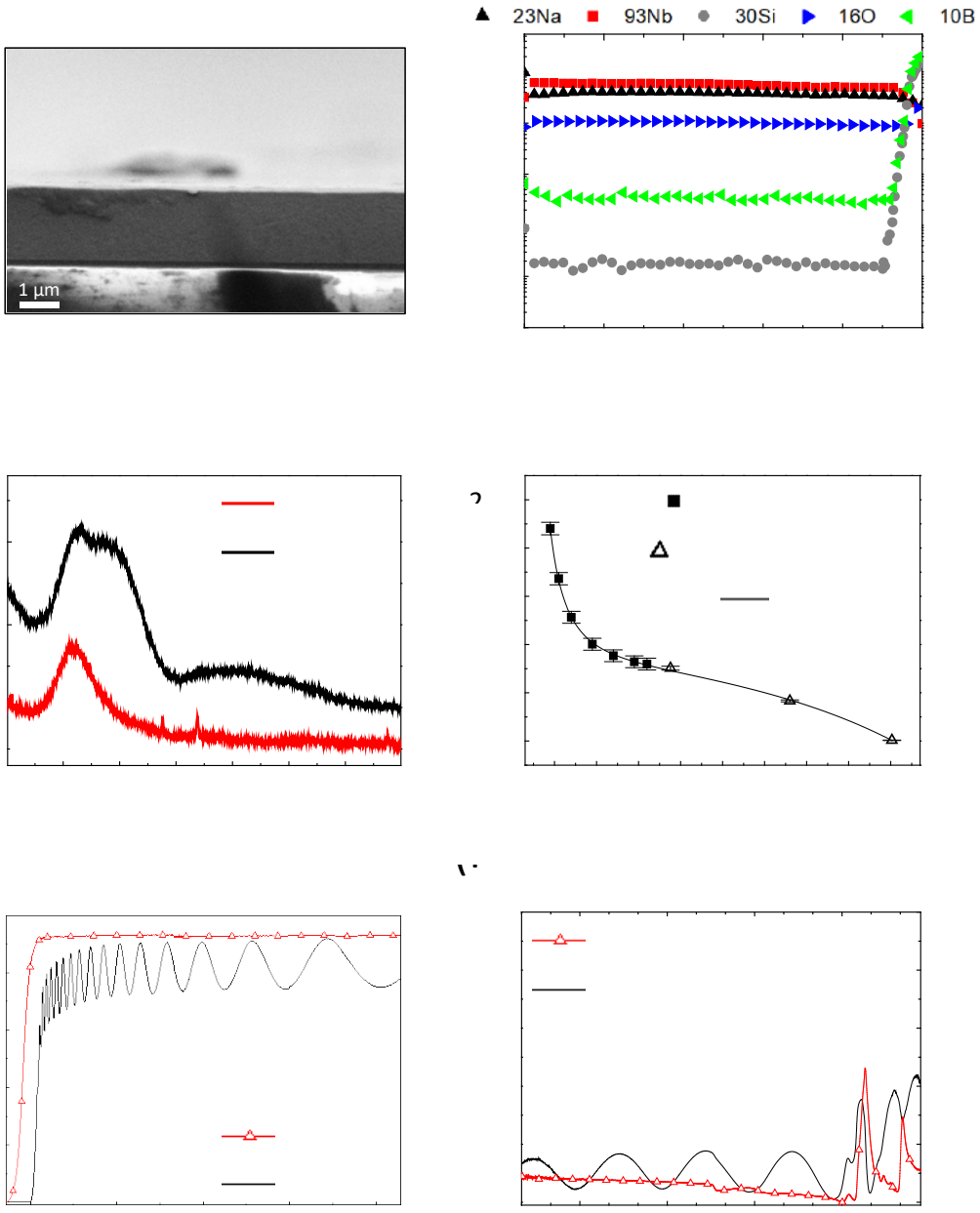

Figure 1. Characterization of the sodo-niobate film: a) Thin film on glass slide cross section viewed by SEM, the scale bar is 1 µm. b) SIMS profile recorded through the depth of the film. Silicon and Boron concentration increase shows that the borosilicate glass substrate interface was reached. c) XRD pattern of the bare borosilicate substrate (in red) and that of the thin film (black) confirming the amorphous nature of both; the three peaks on the substrate's diffractogram originate from the sample holder (aluminum). d) Film refractive index dispersion obtained by a Sellmeier fit on data extracted from two different techniques; on the refractometry measurements (opened squares) the error is within the size of the data point. The transparency window of a 1.4 µm thick film in black: transmission in the visible (e) and reflection in the infra-red (f); as a comparison the substrate's spectra are also presented in red (opened triangles).

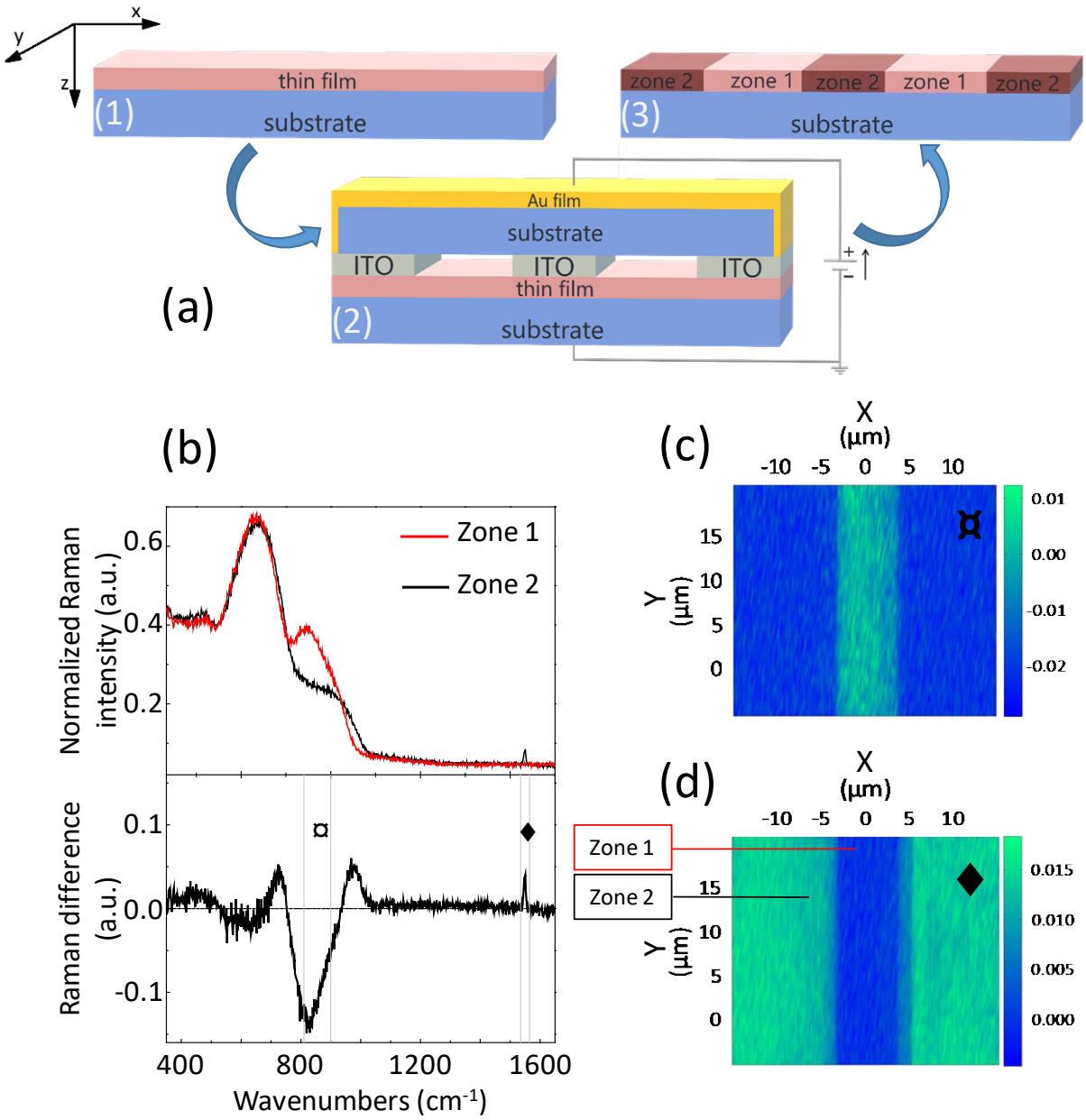

Figure 2. Thermo-electrical micro-imprinting process: a) Schematic of the process: the sodo-niobate thin film is deposited on a borosilicate glass slide (1), and heated while a strong voltage is applied by a structured electrode (in contact with the sample as opposed to some other techniques)[5] (2) and cooled back down before turning the DC field off. This gives rise to two different zones on the post-processed sample (3). b) (top) The characteristic Raman spectra (top) extracted from zone 1 (red) and 2 (black). The spectra have been normalized by the area under the curve. To illustrate evidence of the structural variations of the two regions, the difference Raman spectra is presented (bottom), corresponding to the response in zone 1 (unaffected by poling) subtracted to the poled region in zone 2. c), d) Spatial evolution of two different bands: (c) corresponds Nb-O stretching modes associated with Nb-O^-…Na^+ structural units, and (d) to spectral region illustrating the presence of molecular oxygen attributed to compensation mechanisms occurring during poling.[17]

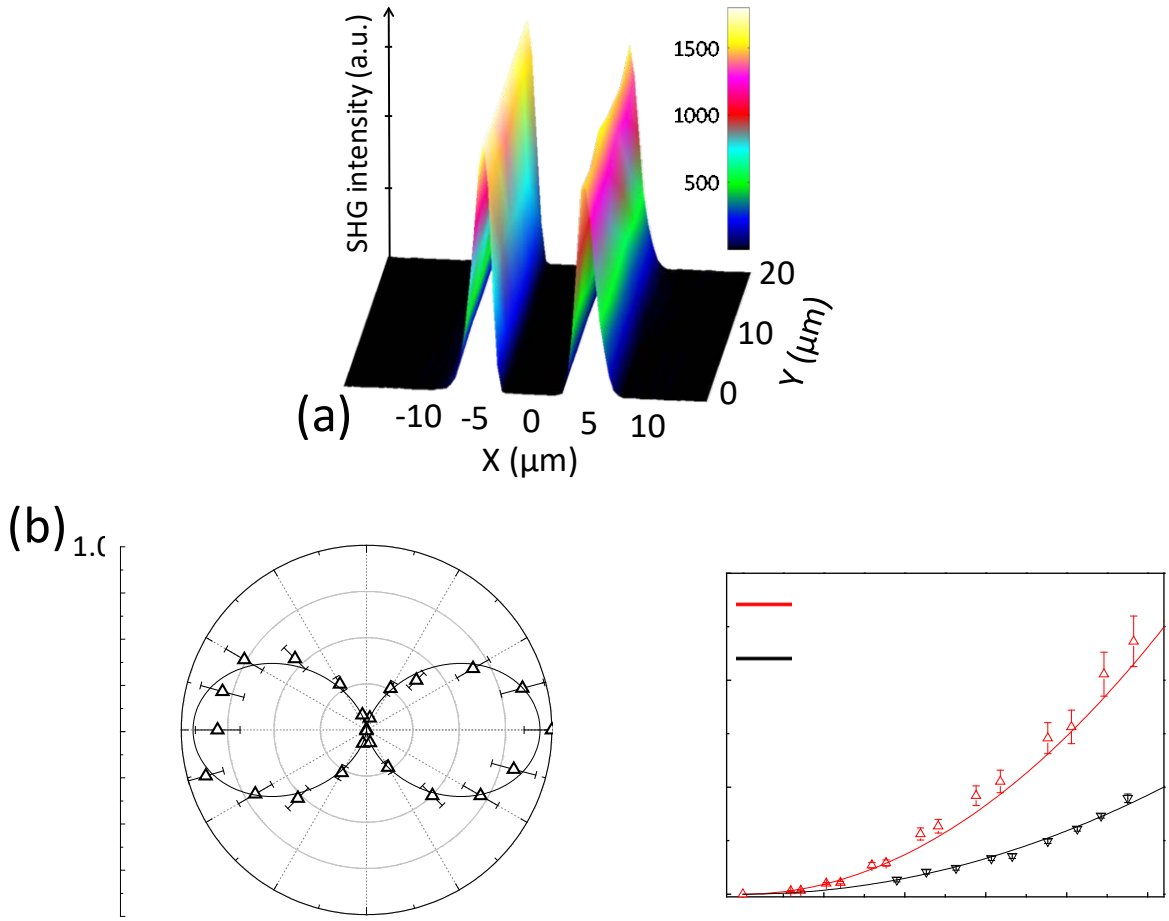

306

307 **Figure 3.** Localization, geometry and magnitude of the induced SONL optical response. a)
308 SHG intensity map realized on the poled film with a linearly polarized light (VV)
309 perpendicular to the imprinted line. b) Normalized SHG intensity as a function of the
310 orientation of the sample (0-180 ° corresponds to the imprinted line perpendicular to the
311 incident light polarization and 90-270 ° parallel). The data were normalized to the maximum
312 value. Repeating the experiment several times allows estimation of error bars to a value of
313 approximately 15 %. A fit with a $\cos^2$ function demonstrates the uniaxial geometry of the
314 response. c) SHG intensity as a function of the linearly polarized incident light power for the
315 thin film (in black – oriented so that the imprinted line is perpendicular to the incident light)
316 and for the LN single crystal (in red – oriented so that the c axis is collinear to the incident
317 light polarization and so that $\chi^{(2)}_{zzz}$ is probed). The error bar was estimated by repeating the
318 measurements. The continuous lines correspond to quadratic fits.
319

A second order nonlinear optical susceptibility is induced by a thermo-electrical imprinting treatment in an amorphous thin film. A magnitude for the $\chi^{(2)}$ of 29 pm/V is measured, this value is the highest ever reported for an amorphous inorganic material. The induced uniaxial anisotropy is localized at the micrometer scale opening the way for new active planar photonic architectures based on amorphous materials.

Nonlinear Optical Materials

Lara Karam, Frédéric Adamietz, Dominique Michau, Claudia Gonçalves, Myungkoo Kang, Rashi Sharma, G. Senthil Murugan, Thierry Cardinal, Evelyn Fargin, Vincent Rodriguez, Kathleen A. Richardson, Marc Dussauze*

Electrically polarized amorphous sodo-niobate film competing with crystalline lithium niobate second order optical response

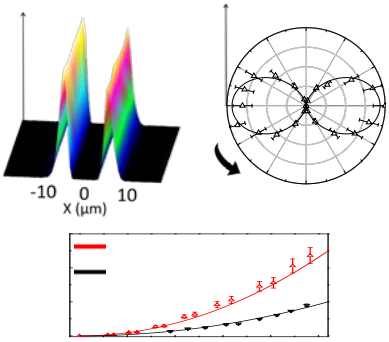

Supporting Information

Electrically polarized amorphous sodo-niobate film competing with crystalline lithium niobate second order optical response

*Lara Karam, Frédéric Adamietz, Dominique Michau, Claudia Gonçalves, Myungkoo Kang, Rashi Sharma, G. Senthil Murugan, Thierry Cardinal, Evelyn Fargin, Vincent Rodriguez, Kathleen A. Richardson, Marc Dussauze**

Thin films deposition:

Thin films were deposited by radio frequency (RF) sputtering in a Leybold L560 system on thoroughly cleaned (in isopropanol and ion sputtered with argon for 4 min) Schott borofloat 33 substrates. The target (75 mm dia.x3 mm thick, 99.9 %pure) of composition 70.8 mol% Nb_2O_5 + 29.2 mol%Na_2O used for that purpose was purchased from Testbourne Ltd. The films were deposited in an argon/oxygen mixture with a gas flow of 47.5 and 2.5 sccm respectively under a pressure of 0.4 Pa at a RF power of 100 W for six hours and fifteen minutes. The deposition rate was of about 0.29 µm/h. The substrates were not heated during the deposition.

Thermal poling:

The thin film on glass substrate, sandwiched between an anode (on the film side) and a silicon wafer at the cathode was heated at a rate of 15 °C/min up to 290 °C under vacuum. A microscope cover was placed between the cathode and the sample to preserve the optical quality on this side. After 10 min under nitrogen flow (6 L/min) to stabilize the temperature, a DC voltage of 1500 V was applied to the sample (at a rate of 375 V/min) and was kept on for 30 min, time after which the sample was brought back to room temperature before the DC voltage was turned off. The anode used consisted of a 100 nm layer of indium tin oxide (ITO) deposited on borosilicate glass. The 10 mmx5 mm electrode has been patterned by laser ablation (see elsewhere for details[17]). In the case of this study straight lines of 10 µm width of ITO have been ablated.

Thin film characterisation prior to poling:

The SEM image of the cross section of the film was performed on a Zeiss Ultra 55 FEG SEM at a working distance of 3.1 mm and under 3 kV. Secondary ion mass spectroscopy (SIMS) measurements were performed by Mikhail Klimov at the Material Characterisation Facility (MCF) at the University of Central Florida (UCF) on PHI Adept 1010 dynamic SIMS system. Xray diffraction (XRD) spectra were acquired by Eric Lebraud at the Insitut de Chimie de la Matière Condensée de Bordeaux (ICMCB) common characterization service the on a PANalytical X'pert PRO MPD diffractometer. Refractive index was measured using a Woollam M2000 ellipsometer in the visible and near infrared (IR) and with a modified Metricon prism coupler (model 2010M) at 1.88, 3.3 and 4.515 µm. Each measurement with the Metricon was repeated ten times and averaged, a reference sample and the bare substrate were also measured prior to the thin film sample. This set of index measurements have been fitted using the following Sellmeier law equation : $\mathbf{n^2 = 1 + \frac{a_1\lambda^2}{\lambda^2 - b_1^2} + \frac{a_2\lambda^2}{\lambda^2 - b_2^2}}$

The fitting curve presented in figure 1(d) have been obtained with the parameter values: (a1=3.12, b1=0.18 µm, a2=1.57, b2=11.0 µm). In more details, one should notice that because our index measurements were not conducted for wavelength higher than 4.5µm, the fitting accuracy for the two terms a_2 and b_2 (linked to the material absorption in the IR domain) is not optimum. Similar theoretical curves could be obtained by adjusting the a_2 term for b_2 values

ranging from 8 to 10 µm. Nevertheless, such analysis accurately depicts the material index dispersion within almost the entire visible-IR transparency range of the niobate films studied. The IR reflectance measurements were performed on a Fourier-transform vacuum spectrometer (Vertex 70V) with a resolution of 4 cm^{-1}. The UV visible transmission spectra were recorded on a Cary 500 (Varian) spectrometer between 200-2300 nm with a 1 nm resolution.

Correlative Raman/SHG confocal microscopy:

Micro-Raman and micro-SHG measurements were recorded in backscattering mode on a modified confocal micro-Raman spectrometer HR800 (Horiba/Jobin Yvon) allowing co-localised Raman and SHG measurements. This correlative microscopy allows for a direct comparison between structural characterization and SONL optical properties. A continuous wave laser operating at 532 nm is used for Raman and a picosecond pulsed laser at 1064 nm is used for micro-SHG measurements. SHG and Raman mapping were realized using a point by point method with a 0.4 µm step in the X direction, and 1 or 4 µm in the Y direction depending on the global map size. Typical resolution used for Raman is 2.5 cm^{-1}. For all measurements the incident laser polarization and the analysed optical Raman and SHG signals were vertically polarized.

SONL optical properties quantification:

To quantify the second order susceptibility using SHG reflection microscopy in confocal mode, we consider that: (i) only the reflected wave originating from the first interface air/dielectric is collected, (ii) one layer of about one wavelength thick contributes to the radiation of the SHG reflected ray as considered by Bloembergen *et al.*[29] Under these assumptions, as the volume of interaction considered is much lower than the coherence length, it is possible to neglect the classical propagation term in the SHG intensity estimation. We can consider the following equation for the SHG reflected intensity, $I_{2\omega}$, as a function of the incident power, I_{ω}:

$$\boldsymbol{I_{2\omega} \sim \frac{(2\omega)^2}{8\varepsilon_0 c^3} \frac{\left|\chi^{(2)}(-2\omega;\omega,\omega)\right|^2}{n_\omega^2 n_{2\omega}} L^2 I_\omega^2}$$

With ε_0: vacuum permittivity

$\boldsymbol{c}$: speed of light in vacuum

ω and $\mathbf{2}\omega$: the incident and second harmonic pulsation

$\boldsymbol{n}_\omega$ and $n_{2\omega}$: the indices at ω and 2ω

L: is the layer thickness contributing to the radiation of the SHG reflected ray. Considering SHG specular reflectance from one unique interface, we assume this layer to be one wavelength thick and to be independent of the materials probed[29].

$\chi^{(2)}$ (- $\mathbf{2}\omega;\omega,\omega$): the second order susceptibility

We have also considered reflection loss for the incident light, this means the actual intensity that participate to the SHG is:

$$I_\omega = \frac{4n_\omega}{(n_\omega + 1)^2} I_\omega^{meas}$$

Where I_ω^{meas} is the measured intensity before the sample's interface.

Therefore, given these approximations, the SHG reflected intensity can be rewritten as:

$$\boldsymbol{I_{2\omega} \sim \frac{4^2(2\omega)^2 L^2}{8\varepsilon_0 c^3} \frac{\left|\chi^{(2)}(-2\omega;\omega,\omega)\right|^2}{(n_\omega + 1)^4 n_{2\omega}} (I_\omega^{meas})^2}$$

If $a_{thin\ film}$ and a_{LN} are respectively the fitting coefficient of the quadratic laws for the thin film and LN single crystal, the final expression for the second order susceptibility of the thin film is:

$$\chi^{(2)}_{thin\ film}(-2\omega;\omega,\omega) = \chi^{(2)}_{LN}(-2\omega;\omega,\omega)\sqrt{\frac{a_{thin\ film}}{a_{LN}}\frac{n_{2\omega}^{thin\ film}\left(n_{\omega}^{thin\ film}+1\right)^4}{n_{2\omega}^{LN}(n_{\omega}^{LN}+1)^4}}$$

Please note that the LN single crystal is not oriented in a phase matching condition. the LN orientation has been chosen to probe only the strongest term of its $\chi^{(2)}$ tensor: $\chi^{(2)}{}_{zzz}$. Similarly, the thin film was oriented to quantify its maximum SHG response, i.e. perpendicular to the imprinted lines along the x-axis in the sample referential, thus probing only the term $\chi^{(2)}{}_{xxx}$.